

Measurement of Spectral Functions of Ultracold Atoms in Disordered PotentialsValentin V. Volchkov,^{1,2} Michael Pasek,^{1,3,†} Vincent Denechaud,^{1,4} Musawwadah Mukhtar,¹Alain Aspect,¹ Dominique Delande,³ and Vincent Josse^{1,*}¹*Laboratoire Charles Fabry, Institut d'Optique, CNRS, Université Paris-Saclay, 91127 Palaiseau cedex, France*²*Max-Planck-Institute for Intelligent Systems, Max-Planck-Ring 4, 72076 Tübingen, Germany*³*Laboratoire Kastler Brossel, UPMC-Sorbonne Universités, CNRS, ENS-PSL Research University, Collège de France, 4 Place Jussieu, 75005 Paris, France*⁴*SAFRAN Sensing Solutions, Safran Tech, Rue des Jeunes Bois, Châteaufort CS 80112, 78772 Magny-les-Hameaux, France* (Received 27 July 2017; published 8 February 2018)

We report on the measurement of the spectral functions of noninteracting ultracold atoms in a three-dimensional disordered potential resulting from an optical speckle field. Varying the disorder strength by 2 orders of magnitude, we observe the crossover from the “quantum” perturbative regime of low disorder to the “classical” regime at higher disorder strength, and find an excellent agreement with numerical simulations. The method relies on the use of state-dependent disorder and the controlled transfer of atoms to create well-defined energy states. This opens new avenues for experimental investigations of three-dimensional Anderson localization.

DOI: [10.1103/PhysRevLett.120.060404](https://doi.org/10.1103/PhysRevLett.120.060404)

Introduction.—The spectral function provides essential information on the energy-momentum relation of one-particle excitations in complex systems. This relation takes a nontrivial form in the presence of random scatterers or interparticle interactions [1]. The direct measurement of the spectral function via angle-resolved photoemission spectroscopy (ARPES) [2] in strongly correlated electronic systems has led to significant progress in the understanding of high- T_c superconductivity [3]. More recently, the ability to measure and exploit spectral functions in ultracold atomic systems has also been widely demonstrated, for instance, using radio-frequency spectroscopy [4,5] to reveal the presence of a pseudogap in strongly interacting Fermi gases [6,7], or to probe the Mott insulator and superfluid regimes of interacting Bose gases in periodic lattices using Bragg spectroscopy [8–10].

In disordered systems, the knowledge of the spectral function is also crucial, from the search of gapless excitations in the Bose glass phase in presence of interactions (see, e.g., Ref. [11]) to the precise investigation of the Anderson quantum phase transition for noninteracting particles [12,13]. In the Anderson localization problem, the spectral function is not only a basic ingredient used in theoretical approaches to predict the position of the mobility edge (the critical energy of the transition) [14], but it is also used as a resource to extract an approximate value of the mobility edge from experimental observations [15–17]. Significant discrepancies observed between the experiments and theoretical analyses [18–20] render the precise measurement of these spectral functions yet more desirable.

In this Letter, we report on the direct measurement of the spectral function at quasi-null momentum of noninteracting

ultracold atoms in continuous three-dimensional (3D) laser speckle disordered potentials. We explore a large range of disorder strengths, from the so-called “quantum” regime of weak disorder (see, e.g., Ref. [21]), where the spectral function is a narrow function whose width gives the inverse lifetime of the initial momentum state, to the so-called “classical” regime of strong disorder, where atoms can be described by a semiclassical wave function and spectral functions converge towards the probability distribution of the disorder [22,23]. The measurements are done both with an attractive (red-detuned) and a repulsive (blue-detuned) laser speckle disorder, the latter case being particularly important since most experimental studies of Anderson localization of ultracold atoms have been done in that configuration. Numerical calculations are in excellent agreement with the experimental results, not only in the marginal regimes of weak and strong disorder, but also in the crossover in between where finding accurate expressions is a theoretical challenge [24–26].

The method is based on a radio-frequency (rf) transfer of atoms at rest in an atomic internal state $|1\rangle$ insensitive to the disorder, to a final internal state $|2\rangle$ sensitive to the disordered potential (see Fig. 1) [27]. The transfer allows us to selectively populate eigenstates of the random potential around the resonant energy $E_f = E_i + \hbar\omega$ set by the rf frequency ω (here $E_{i,f}$ corresponds to the *total* energy of the initial and final states). Because of the finite energy resolution of the transfer, energy levels in the disorder behave as an effective continuum, whose density of states ρ is equal to the density of states averaged over disorder realizations [28]. According to the Fermi golden rule, one can thus define a transfer rate Γ , proportional to the squared

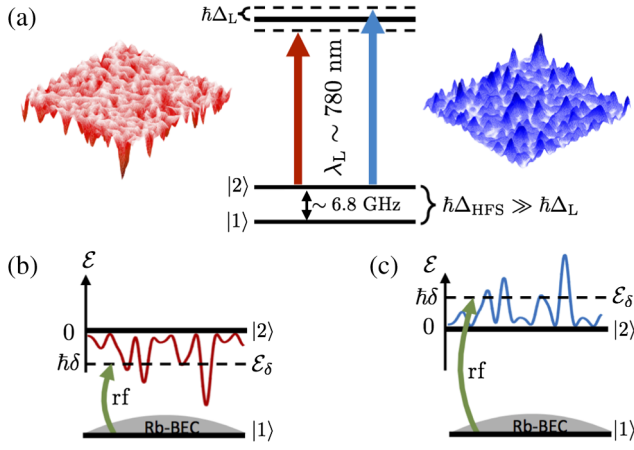


FIG. 1. Measurement scheme of the spectral function using a state-dependent disordered potential. (a) A near-resonant laser speckle field of detuning Δ_L creates either an attractive (red-detuned, $\Delta_L < 0$) or repulsive (blue-detuned, $\Delta_L > 0$) disordered potential on atoms in internal state $|2\rangle$, while the disordered potential experienced by atoms in internal state $|1\rangle$ is negligible, since $\Delta_{\text{HFS}} \gg \Delta_L$. (b) and (c) A radio-frequency field at frequency $\Delta_{\text{HFS}} + \delta$ transfers a small fraction of atoms in a BEC in state $|1\rangle$ to the state $|2\rangle$. The transfer rate measured in this experiment is proportional to the spectral function, according to the Fermi golden rule [see Eq. (1)].

modulus of the transition amplitude from the initial state $|1\rangle$ to the targeted final states, which is directly linked to the spectral function of the disordered potential [see Eq. (1) below]. We start indeed with atoms in a dilute Bose-Einstein condensate (BEC) in a shallow trap, whose wave function is very close to a null momentum state $|\mathbf{k} = 0\rangle$ such that the total energy of the initial state can be taken equal to the internal energy E_1 [28]. The external energy of the final states is then given by $\mathcal{E}_\delta = \hbar\delta$, where $\delta = \omega - \Delta_{\text{HFS}}$ is the rf detuning from the bare resonant frequency corresponding to the hyperfine splitting between the respective internal energies $\Delta_{\text{HFS}}/2\pi = (E_2 - E_1)/h \approx 6.8$ GHz (see Fig. 1). The rf transfer being associated with a negligible momentum change, the transfer rate from state $|1\rangle$ to $|2\rangle$ is thus proportional to the spectral function $A(\mathcal{E}_\delta, \mathbf{k} = 0)$:

$$\Gamma \propto A(\mathcal{E}_\delta, \mathbf{k} = 0) = \overline{\sum_{\alpha} |\langle \mathbf{k} = 0 | \psi_{\alpha} \rangle|^2 \delta(\mathcal{E}_\delta - \mathcal{E}_{\alpha})} \sim \overline{|\langle \mathbf{k} = 0 | \psi_{\delta} \rangle|^2 \rho(\mathcal{E}_\delta)}. \quad (1)$$

Here, $|\psi_{\alpha}\rangle$ corresponds to the eigenstate of energy \mathcal{E}_{α} and $\overline{\dots}$ denotes the averaging over disorder realizations. One can thus determine the spectral function by measuring the transfer rate as a function of the rf detuning δ .

Experiment.—An original feature of the experiment is the realization of a state-dependent disordered potential significant only for the state $|2\rangle$. As sketched in Fig. 1(a), we use a laser close to the hyperfine transition

$F = 2 \leftrightarrow F' = 3$ around the D_2 line of rubidium at wavelength $\lambda_L \sim 780.24$ nm. Tuning the laser at $\Delta_L/2\pi \approx \pm 80$ MHz from the resonance, we create respectively an attractive (red-detuned) or repulsive (blue-detuned) potential for the $F = 2$ state, while the effect is 100 times smaller on the $F = 1$ state since $\Delta_{\text{HFS}} \gg \Delta_L$ [28]. The laser speckle is obtained by passing the laser beam through a diffusive plate [35], which yields a well-characterized disordered potential $V(\mathbf{r})$ [27,28]. The attractive and repulsive cases differ by their probability distribution $P(V) = |V_0|^{-1} \exp[-V/V_0] \Theta(V/V_0)$, with Θ the unit step function, the average value V_0 of the potential being respectively negative or positive. The amplitude of the disorder $|V_0|$ is proportional to the laser intensity, and can be varied over 2 orders of magnitude (see Fig. 2).

In order to obtain a sharp resonance for the $|1\rangle \leftrightarrow |2\rangle$ transition, we use the two “clock states” $|F = 1, m_F = -1\rangle \equiv |1\rangle$ and $|F = 2, m_F = +1\rangle \equiv |2\rangle$, whose energy difference is insensitive (at first order) to magnetic fluctuations at the “magic” magnetic field of $B_0 = 3.23$ G, which we impose on the atoms. The result is a resonance of width about 10 Hz. Note that since the two states have an angular momentum difference $\Delta m_F = 2$, we use a two-photon rf transition, involving a microwave and a rf field [28].

The experiment starts with the realization of a ^{87}Rb -BEC of about $n_1 = 2 \times 10^5$ atoms in the state $|1\rangle$. At the same time, the disordered potential for state $|2\rangle$ is turned on. The microwave and rf fields driving the $|1\rangle \leftrightarrow |2\rangle$ transition are then applied for a time duration t . The rf coupling is weak enough such that the transfer rate Γ can be calculated via the Fermi golden rule as written in Eq. (1) [36–39]. The duration t is chosen short enough, i.e., $\Gamma t \ll 1$, such that only a small fraction of atoms is transferred (a few percents at most). At this short time scale, the population in state $|2\rangle$ grows linearly with time as $n_2(t) \approx n_1(0)\Gamma t$ and the transfer rate is directly obtained by counting the atoms via fluorescence imaging. The spectral function $A(\mathcal{E}_\delta = \hbar\delta, 0)$ is finally obtained by repeating the measurement at various values of the detuning δ . In practice, we adapt the energy resolution, $\Delta\mathcal{E} = \hbar/t$, to the typical energy span of the spectral function for each disorder amplitude, so that it does not affect the observed profile.

Numerical calculations.—The experimental results are compared to the results of numerical calculations that take into account the detailed statistical properties of the laser speckle used in the experiments (see Ref. [28]). The calculations are based on the temporal representation of the spectral function

$$A(\mathcal{E}_\delta, \mathbf{k}) = \frac{1}{\pi\hbar} \text{Re} \int_0^\infty \overline{\langle \mathbf{k} | e^{-iHt/\hbar} | \mathbf{k} \rangle} e^{i\mathcal{E}_\delta t/\hbar} dt, \quad (2)$$

which amounts to evaluating the (disorder-averaged) scalar product between the initial plane-wave excitation $|\mathbf{k}\rangle$ and

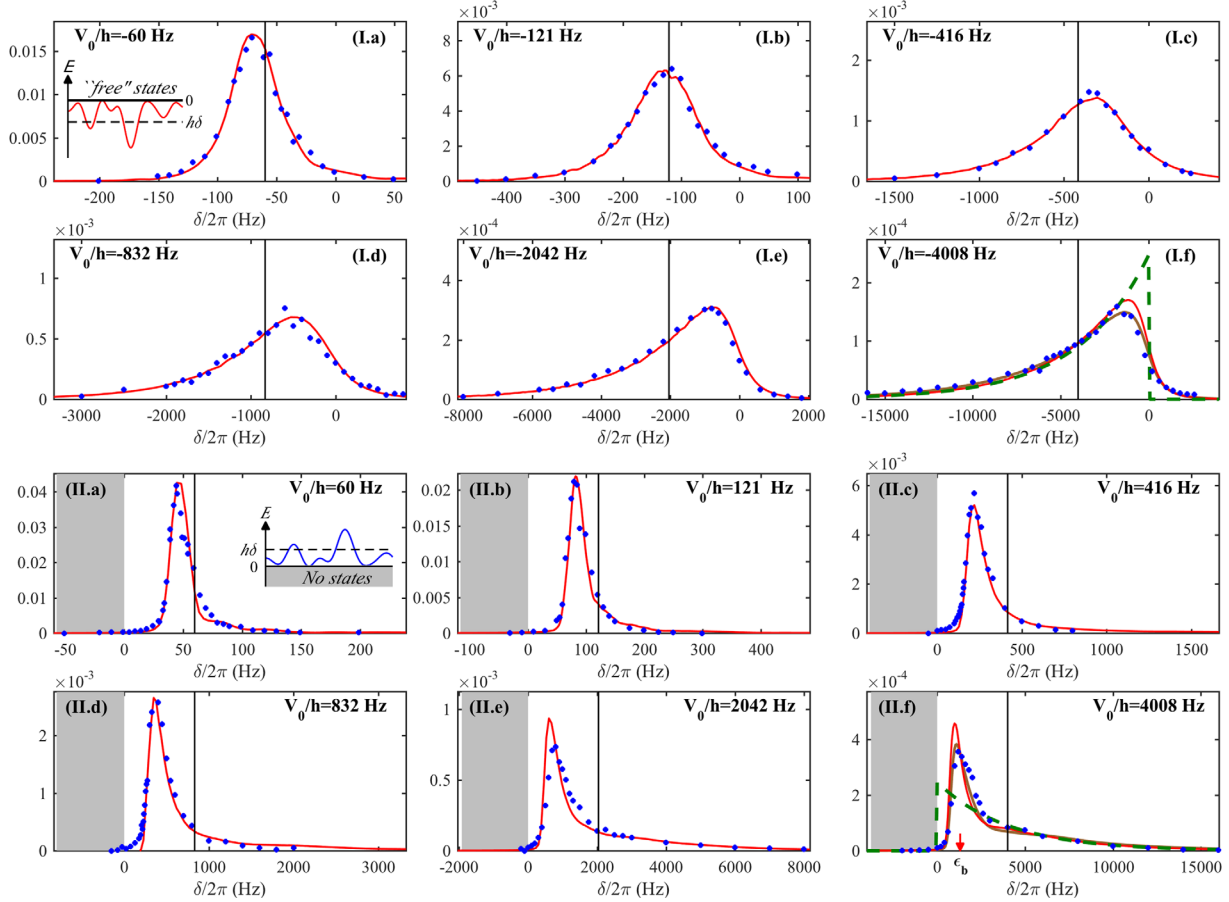


FIG. 2. Measured (blue dots) and numerically calculated (red solid lines) spectral functions $A(\mathcal{E}_\delta = \hbar\delta, \mathbf{k} = 0)$ of atoms in attractive (panel I) or repulsive (panel II) disordered potentials with various amplitudes. Raw numerical results have been convolved by the experimental resolution function, yielding only minor corrections. The solid brown lines in panels (I.f) and (II.f) are the results of numerical computations taking into account the residual effect of disorder in the initial state $|1\rangle$ [28]. In each panel, the black vertical lines indicate the average value V_0/h of the disorder. The small arrow in panel (II.f) indicates the estimated position of the average ground state energy in local minima, $\mathcal{E}_b/h = 1.3$ kHz (see text). Insets in panels (I.a) and (II.a) illustrate the disorder potential for the corresponding configuration. The probability distribution $P(V)$ of the speckle potential is represented as a dashed green curve in panels (I.f) and (II.f).

the time-evolved state $\exp(-iHt/\hbar)|\mathbf{k}\rangle$, with H the disordered Hamiltonian. Our time-propagation algorithm uses an iterative scheme based on the expansion of the time-evolution operator in a series of Chebyshev polynomials of the Hamiltonian [40,41].

Results.—Figure 2 shows the measured spectral functions $A(\mathcal{E}_\delta, 0)$ as well as the results of their numerical calculations, for the cases of attractive (panel I), and repulsive (panel II) disordered potentials with amplitudes $|V_0|$ ranging from 60 Hz to 4 kHz. The area under the experimental curves is normalized in order to allow for a direct comparison with numerical calculations [28]. The disorder strength has been precisely calibrated by adjusting the experimental and numerical curves of panel (I.b), leading to a 14% correction of the amplitude estimated from photometric measurements. This correction factor is then applied to all other measurements. The agreement is excellent over the whole range of disorder amplitudes. Note

that, in contrast with numerical calculations, no disorder-averaging was necessary for the experimental data. This is due both to the finite experimental energy resolution that provides an effective averaging over many energy states, and to the very large expansion of the initial BEC that “samples” efficiently the disordered potential.

In the attractive case (Fig. 2, panel I), we observe a smooth crossover from the weak disorder regime [panel (I.a)], where the spectral function is relatively narrow, symmetrical and centered closed to the averaged disorder amplitude V_0 , to the strong disorder regime [panel (I.f)] where it becomes strongly asymmetrical. These two marginal regimes can be understood by introducing an important energy scale of the problem, the correlation energy, $\mathcal{E}_\sigma = \hbar^2/m(\sigma_\perp^2\sigma_\parallel)^{2/3}$ [20] associated with the finite spatial correlations lengths of the disordered potential. Here, m is the atomic mass, while σ_\perp and σ_\parallel are, respectively, the transverse and longitudinal correlation lengths of the

anisotropic laser speckle intensity [28]. For our experiment $\sigma_{\perp} \sim 0.306$ and $\sigma_{\parallel} \sim 1.45 \mu\text{m}$ leading to $\mathcal{E}_{\sigma}/\hbar \approx 441$ Hz.

In the quantum regime [$|V_0| \ll \mathcal{E}_{\sigma}$, see panel (I.a)], the amplitude of the disordered potential is too small to support bound states on the typical size $\sigma = (\sigma_{\perp}^2 \sigma_{\parallel})^{1/3}$ of a speckle grain. Atoms with an energy of the order of $|V_0|$ have a large de Broglie wavelength compared to σ and their wave function extends over many speckle grains [see Fig. 3(a)]. This leads to a smoothing of the disordered potential (see, e.g., Refs. [42,43]), whose rescaled effective amplitude corresponds to the width of the spectral function. Alternatively, a perturbative approach of scattering allows us to interpret this width as the inverse lifetime \hbar/τ_S , where τ_S is the elastic scattering time, of the initial state $|\mathbf{k} = 0\rangle$ [44]. This approach predicts a Lorentzian shape for the spectral function, with a width $\sim \pi V_0^2/\mathcal{E}_{\sigma}$ [21,25,43]. This explains the quasi-Lorentzian shape shown in panel (I.a).

In the classical regime [$|V_0| \gg \mathcal{E}_{\sigma}$, see panel (I.f)] the situation is the opposite: atoms with an energy of the order of $|V_0|$ have a de Broglie wavelength small compared to σ . The corresponding wave functions have short spatial oscillations, except around the turning points r_j selected by the resonance condition $V(r_j) = \hbar\delta$, where atoms bounce classically on the disordered potential [see Fig. 3(b)]. The overlap with the uniform initial state $|\mathbf{k} = 0\rangle$ is thus negligible except at these positions (the so-called ‘‘Franck-Condon principle’’). The transfer rate—or, equivalently, the spectral function—is then a probe of the points where $V = \hbar\delta$, i.e., the probability distribution $P(V)$. This property was used in Ref. [27] to estimate the disorder amplitude V_0 . Alternatively, it can be retrieved using the formal expression of the spectral function $A(\mathcal{E}, \mathbf{k}) = \overline{\langle \mathbf{k} | \delta(\mathcal{E} - H) | \mathbf{k} \rangle}$ [28]. Neglecting the kinetic energy term when $|V_0| \gg \mathcal{E}_{\sigma}$, it yields directly

$A(\mathcal{E}, \mathbf{k} = 0) = P(V)$ (see, e.g., Ref. [22]). Consistently, we observe that the spectral function converges at strong disorder towards the probability distribution of the speckle potential [dashed green curve in panel (I.f)]. However, the de Broglie wavelength of atoms remains large around $|\mathcal{E}_{\delta}| \sim 0$, so that the spectral function smoothes out the sharp discontinuity of the potential distribution.

If we consider now the repulsive case (panel II), the potential distribution is bounded from below with no state in the negative energy range (gray area). This has two consequences. First, the spectral function is strictly zero for negative energy. Second, in the strong disorder regime, the low energy states that are supported by local minima of the disordered potential lead to an accumulation of states around the averaged ground state harmonic oscillator energy $\mathcal{E}_b \sim \sqrt{V_0 \mathcal{E}_{\sigma}}$ [22,23]. This results in a pronounced and narrow peak in the spectral function, which is clearly visible in panel (II.f) around the energy \mathcal{E}_b (within 30%). While the qualitative explanation was given in the strong-disorder limit, let us note that the peak is present in all the spectral functions shown in panel II. At the lowest disorder amplitude (II.a), it results in a very narrow spectral function, significantly narrower than for the attractive case (I.a) and far from perturbative predictions. This behavior is fully consistent with the strong departure from the perturbative Born prediction observed in the direct measurement of the elastic scattering time τ_S (which is related to the inverse of the spectral function’s width as discussed above) for the same disorder configuration [45]. These observations emphasize the difficulties encountered when approximate theories of Anderson localization use perturbative expressions of the spectral function as a resource (see, e.g., Refs. [21,24,25]).

Conclusion.—We have demonstrated a method that uses a state dependent disordered potential to probe the spectral functions of ultracold atoms in 3D laser speckle potentials. This allowed us to study the crossover from the quantum to the classical regime, the behavior being significantly different for red-detuned or blue-detuned laser speckles. In the latter case, a pronounced peak attributed to lowest bound states in potential minima is observed, resulting in strong deviations from what we would expect using a weak-scattering perturbative approach. The present method, which yields the spectral function around zero momentum, could easily be generalized to finite values of \mathbf{k} by, for instance, using stimulated Raman transitions effected by two laser beams whose angle allows one to select the desired value of \mathbf{k} [28,46]. Besides the measurement of the spectral functions, a key feature of the presented method is the controlled transfer of atoms to well-defined energy states in the disorder, the targeted energy being chosen by the resonance condition. It opens the possibility to probe the 3D Anderson transition, via a subsequent wave packet expansion, with an unprecedented energy resolution compared to earlier experimental attempts [15–17]. The interest

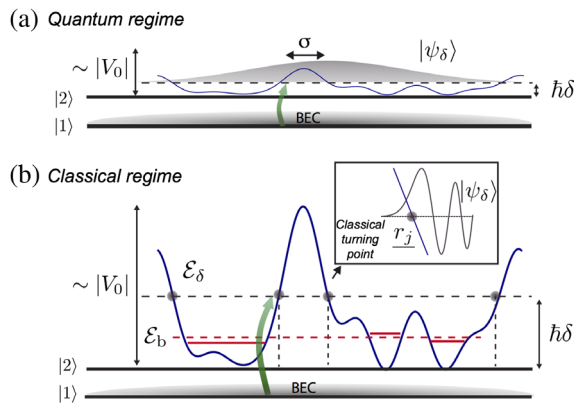


FIG. 3. Schematics of the two marginal regimes of spectral functions of noninteracting atoms in disordered potentials (here shown for the blue-detuned case). (a) Weak disorder $|V_0| \ll \mathcal{E}_{\sigma}$, quantum regime; (b) Strong disorder $|V_0| \gg \mathcal{E}_{\sigma}$, classical regime. \mathcal{E}_b corresponds to the average energy of the ground states in local potential minima (see text) for blue-detuned laser speckle disordered potential.

ranges from the precise location of the mobility edge in such spatially continuous disordered potentials [19,20] to the investigation of the critical regime [47] and the eventual observation of multifractality [48]. Last, the scheme could be implemented in a “reversed way,” as proposed in Refs. [4,49], where the ultracold atomic sample under investigation is in the disorder-sensitive state while the resonant transfer is driven to the “free” state. This configuration could be used to probe the complex excitation spectra of interacting and disordered quantum gases [4], for instance, to reveal the predicted gapless excitation spectrum in the Bose glass phase [50,51].

This work was supported by ERC (Advanced Grant “Quantatop”), the Institut Universitaire de France, the Region Ile-de-France in the framework of DIM Nano-K (project QUGASP), the French Ministry of Research and Technology (ANRT) through a CIFRE/DGA grant for V. D. and the project ANR-12-BS04-0022-01, and the EU-H2020 research and innovation program (Grant No. 641122-QUIC and Marie Skłodowska-Curie Grant No. 655933). The authors were granted access to the HPC resources of TGCC under the allocation 2016-057644 made by GENCI (“Grand Equipement National de Calcul Intensif”).

V. V. and M. P. contributed equally to this work.

*Corresponding author.

vincent.josse@institutoptique.fr

†Present address: Collège de France, 11 place Marcelin Berthelot, 75005 Paris, France.

- [1] H. Bruus and K. Flensberg, *Many-Body Quantum Theory in Condensed Matter Physics* (Oxford University Press, Oxford, England, 2004).
- [2] A. Damascelli, Probing the electronic structure of complex systems by ARPES, *Phys. Scr.* **T109**, 61 (2004).
- [3] A. Damascelli, Z. Hussain, and Z.-X. Shen, Angle-resolved photoemission studies of the cuprate superconductors, *Rev. Mod. Phys.* **75**, 473 (2003).
- [4] T.-L. Dao, A. Georges, J. Dalibard, C. Salomon, and I. Carusotto, Measuring the One-Particle Excitations of Ultracold Fermionic Atoms by Stimulated Raman Spectroscopy, *Phys. Rev. Lett.* **98**, 240402 (2007).
- [5] J. T. Stewart, J. P. Gaebler, and D. S. Jin, Using photoemission spectroscopy to probe a strongly interacting Fermi gas, *Nature (London)* **454**, 744 (2008).
- [6] J. P. Gaebler, J. T. Stewart, T. E. Drake, D. S. Jin, A. Perali, P. Pieri, and G. C. Strinati, Observation of pseudogap behaviour in a strongly interacting Fermi gas, *Nat. Phys.* **6**, 569 (2010).
- [7] M. Feld, B. Fröhlich, E. Vogt, M. Koschorreck, and M. Köhl, Observation of a pairing pseudogap in a two-dimensional Fermi gas, *Nature (London)* **480**, 75 (2011).
- [8] D. Clément, N. Fabbri, L. Fallani, C. Fort, and M. Inguscio, Exploring Correlated 1D Bose Gases from the Superfluid to the Mott-Insulator State by Inelastic Light Scattering, *Phys. Rev. Lett.* **102**, 155301 (2009).
- [9] P. T. Ernst, S. Götze, J. S. Krauser, K. Pyka, D.-S. Lühmann, D. Pfannkuche, and K. Sengstock, Probing superfluids in optical lattices by momentum-resolved Bragg spectroscopy, *Nat. Phys.* **6**, 56 (2010).
- [10] N. Fabbri, S. D. Huber, D. Clément, L. Fallani, C. Fort, M. Inguscio, and E. Altman, Quasiparticle Dynamics in a Bose Insulator Probed by Interband Bragg Spectroscopy, *Phys. Rev. Lett.* **109**, 055301 (2012).
- [11] C. D’Errico, E. Lucioni, L. Tanzi, L. Gori, G. Roux, I. P. McCulloch, T. Giamarchi, M. Inguscio, and G. Modugno, Observation of a Disordered Bosonic Insulator from Weak to Strong Interactions, *Phys. Rev. Lett.* **113**, 095301 (2014).
- [12] P. W. Anderson, Absence of diffusion in certain random lattices, *Phys. Rev.* **109**, 1492 (1958).
- [13] E. Abrahams, *50 Years of Anderson Localization* (World Scientific, Singapore, 2010).
- [14] D. Vollhardt and P. Wölfle, in *Electronic Phase Transitions*, edited by W. Hanke and Y. V. Kopaev (Elsevier, New York, 1992), Vol. 1, p. 1.
- [15] S. S. Kondov, W. R. McGehee, J. J. Zirbel, and B. DeMarco, Three-dimensional Anderson localization of ultracold matter, *Science* **334**, 66 (2011).
- [16] F. Jendrzejewski, A. Bernard, K. Müller, P. Cheinet, V. Josse, M. Piraud, L. Pezze, L. Sanchez-Palencia, A. Aspect, and P. Bouyer, Three-dimensional localization of ultracold atoms in an optical disordered potential, *Nat. Phys.* **8**, 398 (2012).
- [17] G. Semeghini, M. Landini, P. Castilho, S. Roy, G. Spagnolli, A. Trenkwalder, M. Fattori, M. Inguscio, and G. Modugno, Measurement of the mobility edge for 3D Anderson localization, *Nat. Phys.* **11**, 554 (2015).
- [18] M. Piraud, L. Pezzé, and L. Sanchez-Palencia, Matter wave transport and Anderson localization in anisotropic three-dimensional disorder, *Europhys. Lett.* **99**, 50003 (2012).
- [19] E. Fratini and S. Pilati, Anderson localization of matter waves in quantum-chaos theory, *Phys. Rev. A* **91**, 061601 (2015).
- [20] M. Pasek, G. Orso, and D. Delande, Anderson Localization of Ultracold Atoms: Where is the Mobility Edge?, *Phys. Rev. Lett.* **118**, 170403 (2017).
- [21] R. C. Kuhn, O. Sigwarth, C. Miniatura, D. Delande, and C. A. Müller, Coherent matter wave transport in speckle potentials, *New J. Phys.* **9**, 161 (2007).
- [22] M. I. Trappe, D. Delande, and C. A. Müller, Semiclassical spectral function for matter waves in random potentials, *J. Phys. A* **48**, 245102 (2015).
- [23] T. Prat, N. Cherroret, and D. Delande, Semiclassical spectral function and density of states in speckle potentials, *Phys. Rev. A* **94**, 022114 (2016).
- [24] A. Yedjour and B. A. van Tiggelen, Diffusion and localization of cold atoms in 3D optical speckle, *Eur. Phys. J. D* **59**, 249 (2010).
- [25] M. Piraud, L. Pezzé, and L. Sanchez-Palencia, Quantum transport of atomic matter waves in anisotropic two-dimensional and three-dimensional disorder, *New J. Phys.* **15**, 075007 (2013).
- [26] M. Pasek, Z. Zhao, D. Delande, and G. Orso, Phase diagram of the three-dimensional Anderson model for short-range speckle potentials, *Phys. Rev. A* **92**, 053618 (2015).

- [27] D. Clément, A. F. Varón, J. A. Retter, L. Sanchez-Palencia, A. Aspect, and P. Bouyer, Experimental study of the transport of coherent interacting matter-waves in a 1D random potential induced by laser speckle, *New J. Phys.* **8**, 165 (2006).
- [28] See Supplemental Material at <http://link.aps.org/supplemental/10.1103/PhysRevLett.120.060404>, which includes Refs. [29–34], for details on the transfer protocol (theoretical description and experimental implementations), the laser speckle disordered potential (realization, characterization, and simulation), and the numerical procedure.
- [29] F. Jendrzejewski, K. Müller, J. Richard, A. Date, T. Plisson, P. Bouyer, A. Aspect, and V. Josse, Coherent Backscattering of Ultracold Atoms, *Phys. Rev. Lett.* **109**, 195302 (2012).
- [30] D. M. Harber, H. J. Lewandowski, J. M. McGuirk, and E. A. Cornell, Effect of cold collisions on spin coherence and resonance shifts in a magnetically trapped ultracold gas, *Phys. Rev. A* **66**, 053616 (2002).
- [31] M. Egorov, B. Opanchuk, P. Drummond, B. V. Hall, P. Hannaford, and A. I. Sidorov, Measurement of s-wave scattering lengths in a two-component Bose-Einstein condensate, *Phys. Rev. A* **87**, 053614 (2013).
- [32] L. J. LeBlanc and J. H. Thywissen, Species-specific optical lattices, *Phys. Rev. A* **75**, 053612 (2007).
- [33] J. Richard, Ph.D. thesis, Université Paris-Saclay, 2015.
- [34] T.-L. Dao, I. Carusotto, and A. Georges, Probing quasiparticle states in strongly interacting atomic gases by momentum-resolved Raman photoemission spectroscopy, *Phys. Rev. A* **80**, 023627 (2009).
- [35] J. W. Goodman, *Speckle Phenomena in Optics: Theory and Applications* (Dover, New York, 2007).
- [36] G. M. Moy, J. J. Hope, and C. M. Savage, Born and Markov approximations for atom lasers, *Phys. Rev. A* **59**, 667 (1999).
- [37] M. W. Jack, M. Naraschewski, M. J. Collett, and D. F. Walls, Markov approximation for the atomic output coupler, *Phys. Rev. A* **59**, 2962 (1999).
- [38] F. Gerbier, P. Bouyer, and A. Aspect, Quasicontinuous Atom Laser in the Presence of Gravity, *Phys. Rev. Lett.* **86**, 4729 (2001).
- [39] G. Grynberg, A. Aspect, and C. Fabre, *Complement 1A in: Introduction to quantum optics: from the semi-classical approach to quantized light* (Cambridge University Press, Cambridge, England, 2010).
- [40] S. Roche and D. Mayou, Conductivity of Quasiperiodic Systems: A Numerical Study, *Phys. Rev. Lett.* **79**, 2518 (1997).
- [41] H. Fehske, J. Schleede, G. Schubert, G. Wellein, V. S. Filinov, and A. R. Bishop, Numerical approaches to time evolution of complex quantum systems, *Phys. Lett. A* **373**, 2182 (2009).
- [42] B. I. Shklovskii, Superfluid-insulator transition in “Dirty” ultracold Fermi gas, *Semiconductors* **42**, 909 (2008).
- [43] B. Shapiro, Cold atoms in the presence of disorder, *J. Phys. A* **45**, 143001 (2012).
- [44] E. Akkermans and G. Montambaux, *Mesoscopic Physics of Electrons and Photons* (Cambridge University Press, Cambridge, England, 2007).
- [45] J. Richard, L.-K. Lim, V. Denechaud, V. Volchkov, F. Jendrzejewski, A. Aspect, L. Sanchez-Palencia, and V. Josse (to be published).
- [46] M. Kozuma, L. Deng, E. W. Hagley, J. Wen, R. Lutwak, K. Helmerson, S. L. Rolston, and W. D. Phillips, Coherent Splitting of Bose-Einstein Condensed Atoms with Optically Induced Bragg Diffraction, *Phys. Rev. Lett.* **82**, 871 (1999).
- [47] K. Slevin and T. Ohtsuki, Critical exponent for the Anderson transition in the three-dimensional orthogonal universality class, *New J. Phys.* **16**, 015012 (2014).
- [48] A. Rodriguez, L. J. Vasquez, K. Slevin, and R. A. Römer, Critical Parameters from a Generalized Multifractal Analysis at the Anderson Transition, *Phys. Rev. Lett.* **105**, 046403 (2010).
- [49] L. Pezzé and L. Sanchez-Palencia, Localized and Extended States in a Disordered Trap, *Phys. Rev. Lett.* **106**, 040601 (2011).
- [50] T. Giamarchi and H. J. Schulz, Anderson localization and interactions in one-dimensional metals, *Phys. Rev. B* **37**, 325 (1988).
- [51] M. P. A. Fisher, P. B. Weichman, G. Grinstein, and D. S. Fisher, Boson localization and the superfluid-insulator transition, *Phys. Rev. B* **40**, 546 (1989).